

# Small Localized Black Holes in Braneworld

— *Formulation and Numerical method* —

Hideaki Kudoh<sup>1,\*</sup>, Takahiro Tanaka<sup>2,†</sup> and Takashi Nakamura<sup>1‡</sup>

<sup>1</sup> Department of Physics, Kyoto University, Kyoto 606-8502, Japan

<sup>2</sup> Yukawa Institute for Theoretical Physics, Kyoto University, Kyoto 606-8502, Japan

Black holes localized on a 3-brane in Randall-Sundrum infinite braneworld have not been constructed without a naked singularity under asymptotic AdS boundary condition. The problem to find a static black hole solution is reduced to a boundary value problem, and we have solved it by means of numerical method. We construct black hole solutions whose horizon radius is small compared to the bulk curvature scale, and quantitatively analyze the behavior of the numerically obtained black hole solutions, focusing on the thermodynamic quantities. The shape of the small black hole exhibits a flattened geometry in the bulk, and the thermodynamic relations indicate that the localized black hole solutions show a smooth transition from five-dimensional Schwarzschild black hole, which is the solution in the limit of small horizon radius, to solutions which have thermodynamic character similar to four-dimensional Schwarzschild black hole. However, it becomes difficult to find black hole solutions as its horizon radius increases, and we could not construct large black holes whose horizon radius is greater than the bulk curvature scale.

PACS numbers: 04.50.+h, 04.70.Bw, 04.70.Dy

## I. INTRODUCTION

Higher dimensional black holes have been considered for a long time as purely theoretical applications motivated by higher dimensional theories, such as string theory. However, recent developments in the scenario of large extra dimensions [1] brought us a new interest in such black holes. In the braneworld scenario an interesting possibility of black hole production at collider was pointed out [2, 3]. There is another type of braneworld models proposed by Randall and Sundrum (RS) [4, 5]. In these models, the geometry warped in the direction of an extra dimension is used to explain the hierarchy between TeV scale and Planck scale, and to realize four-dimensional gravity effectively on the 3-brane. Also in the context of RS models, the higher dimensional black holes may play an important role. These so-called braneworld scenarios provide us new and interesting situations to investigate higher dimensional black holes.

In the model of large extra dimensions, a physically meaningful sequence of black hole solutions will be obtained as a slight modification of the higher dimensional Kerr black hole [6] (or more simply the Schwarzschild black hole [7, 8, 9]) if the horizon radius is sufficiently small compared to the extension of extra dimensions and the self-gravity due to periodic boundary is weak. As another sequence, there are the black string solutions. A black string is in general unstable to linear perturbations with long wavelength in the direction along the string, which is called Gregory-Laflamme instability [10]. (A stability analysis of black strings is also found in Ref. [11].) Therefore a black string is unstable when the horizon radius of the black string is sufficiently small compared to the extension of the extra dimension. For such a small black hole, the former sequence is expected to be stable. For RS models, since the 3-brane has tension, it is more difficult to find black hole solutions. Trivial black string solution is allowed also in these models, and it becomes unstable in the same way. There are many discussions about black hole in this model and some black hole solutions have been considered by several authors [12, 13, 14, 15, 16, 17, 18, 19, 20, 21, 22, 23, 24, 25, 26, 27]. A strategy to construct a black hole solution is to assume an induced metric on the 3-brane as an *initial data*, and extend it to the bulk analytically or numerically. This method generally results in a naked singularity in the bulk since there is no guarantee that the induced metric assumed as a boundary condition is compatible with a regular geometry. If we randomly specify the boundary metric on the 3-brane, almost all solutions develop a naked singularity. After all, any realistic black hole solutions, which are stable and have no naked singularity, have not been known so far, and finding them is an interesting open question of nonlinear gravity in the braneworld.

Shape of black holes in the RS infinite braneworld [5] is conjectured based on the Gregory-Laflamme instability [25].

---

\*Electronic address: kudoh@yukawa.kyoto-u.ac.jp

†Electronic address: tanaka@yukawa.kyoto-u.ac.jp

‡Electronic address: takashi@yukawa.kyoto-u.ac.jp

It was argued that an unstable black string will be pinched into many black holes. Besides black holes in the bulk, there will be a black hole that is localized on the 3-brane. We can imagine this as a black hole bound to a domain wall if the 3-brane is realized by a domain wall [28]. An exact solution representing a localized black hole is known in 4D braneworld model, which we call in this paper Emparan-Horowitz-Myers (EHM) solution [29]. However the corresponding solution in the original 5D braneworld model has not been discovered. While the localization of black hole was inspired by the classical instability of black string, the anticipated dynamics of pinching off the horizon is questioned by Horowitz and Maeda [30]. Recently, Wiseman discovered non-uniform black string by numerical calculation [31]. The obtained solutions are likely to be unstable, but they are suggestive as a missing link between the localized black hole and the black string.

There is another discussion anticipating the absence of the localized black hole. It was first conjectured in Ref. [33] based on an extensive use of the AdS/CFT correspondence that localized black holes may *classically* evaporate in the 5D RS model. If this conjecture is correct, there will be no static solution of black hole that is asymptotically AdS and is sufficiently large compared with the bulk curvature length. As there exist several solar mass black hole candidates stably, this evaporation sets an interesting constraint on the allowed value of the bulk curvature scale. Further discussion motivated by a no-go theorem [32], and a more explicit study on showing that the existence of the EHM solution does not contradict with this conjecture found in Ref. [34].

On the other hand, however, recovery of 4D gravity on the 3-brane is so successful in the RS models. It was shown that 4D Einstein gravity is approximately recovered in linear perturbations [35, 36, 37, 38, 39] and also in the second order perturbations [40, 41, 42, 43]. Moreover, even in the case of highly relativistic star, 4D Einstein gravity was numerically shown to be a good approximation [44]. Hence, there are also good reasons to support the existence of black hole solutions localized on the 3-brane. If it is the case, the black holes will be produced as a result of gravitational collapse on the brane. The exterior field will settle down to a static state at late times, although it is not static during the collapse on the brane even in a spherical case [32].

The present paper explores the problem of black hole in the RS infinite braneworld [5]. We consider a numerical construction of black hole solution in this model. The method we use in this paper is based on a scheme developed by Wiseman [44]. Our method does not require any assumptions for the induced metric on the 3-brane. We solve Einstein equations numerically under the boundary conditions determined by physical requirements. We will find small black hole solutions, whose horizon radius is smaller than the AdS curvature radius, although large black hole solutions have not been discovered.

In the next section, we explain our method formulating the problem to be suitable for numerical calculation, and the boundary conditions are also discussed. The results of numerical calculations are shown in Section III, where we discuss thermodynamic relations obtained by analyzing our solutions. In section IV, we summarize and discuss our results. Relation between our numerical solutions and the conjecture based on the AdS/CFT is also discussed there.

## II. FORMULATION AS A BOUNDARY VALUE PROBLEM

### A. Conformal transformation

To obtain black hole solutions in RS infinite braneworld model, it is crucial to formulate the problem as a boundary value problem without assuming any artificial boundary conditions. We follow and develop the numerical method developed in Ref. [44] (see also [31]). What we want to find is a static black hole solution that is localized on the brane. For simplicity, we further restrict our attention to the configuration with 5D axial symmetry (4D spherical symmetry). Under the static and axisymmetric assumption, the metric depends only on the radial coordinate  $r$  and the coordinate  $z$  in the direction of the extra dimension. Then, without loss of generality, the metric can be written as

$$ds^2 = \frac{\ell^2}{z^2} (-T^2 dt^2 + e^{2R}(dr^2 + dz^2) + r^2 e^{2C} d\Omega^2), \quad (1)$$

where  $d\Omega^2 = d\theta^2 + \sin^2 \theta d\phi^2$  represents the line element on a unit 2-sphere. The cosmological constant in the bulk is related to the bulk curvature length  $\ell$  by  $\Lambda = -6/\ell^2$ . If we set  $T = 1$  and  $R = C = 0$ , this metric becomes the AdS metric in the Poincaré coordinates. Since we consider a localized black hole, polar coordinates

$$\begin{aligned} r &= \rho \sin \chi, \\ z &= \ell + \rho \cos \chi, \\ \xi &= \chi^2, \end{aligned} \quad (2)$$

are more convenient. Then, we have

$$dr^2 + dz^2 = d\rho^2 + \frac{\rho^2}{4\xi} d\xi^2. \quad (3)$$

The angular coordinate  $\xi$  is useful to treat the coordinate singularity at  $\chi = 0$  numerically since the singularity becomes milder in  $\xi$  coordinate as we will see later [45].

For numerical calculations, it is convenient if the boundaries are located on lines where one of the coordinates is constant. This can be achieved in general by using the residual gauge degrees of freedom. The metric form (1) has the gauge degrees of freedom of conformal transformations in the two dimensional space spanned by  $r$  and  $z$ . For our present purpose, it is convenient to use the conformal polar coordinates  $(\zeta, \chi)$ , where  $\zeta = \log \rho$ . Using these coordinates, we have  $dr^2 + dz^2 = \rho^2(d\zeta^2 + d\chi^2)$ . For the conformal transformation  $\zeta' = f(\zeta, \chi)$  and  $\chi' = g(\zeta, \chi)$ ,  $f$  and  $g$  satisfy the Cauchy-Riemann relations. With a function  $\psi(\zeta, \chi)$ , we have

$$d\zeta'^2 + d\chi'^2 = \psi(\zeta, \chi) (d\zeta^2 + d\chi^2). \quad (4)$$

We can use these conformal degrees of freedom to deform the shape of the boundaries. From the Cauchy-Riemann relations,  $g$  (and also  $f$ ) satisfies Laplace equation, and thus  $g$  is completely determined by specifying its boundary conditions. Suppose we set  $g = 0$  on the axis and  $g = \pi/2$  on the brane, and impose Neumann boundary conditions on the horizon boundary and the asymptotic boundary. The transformation  $f$  is determined by integrating the Cauchy-Riemann relations. The Neumann conditions for  $g$  on the horizon boundary and on the asymptotic boundary guarantee the constancy of  $f$  on these two boundaries. In this manner, we can generally find a conformal transformation that transforms each boundary to a constant coordinate line. Here we note that  $f$  is uniquely determined up to adding a constant. Hence, the difference of the value of  $\zeta'$  between two points cannot be changed arbitrarily. We therefore do not have a degree of freedom to change the ratio  $\rho/\rho_h$  for a given solution. To conclude, the location of the event horizon can be transformed to be

$$\rho|_{\text{horizon}} = \text{const.} = \rho_h, \quad (5)$$

and the brane can be placed at  $z = \ell$  [36].

## B. Elliptic equations and constraint equations

Let us consider the elliptic equations and constraint equations that we solve. From the five dimensional vacuum Einstein equations,  $\mathcal{G}_\nu^\mu := R_\nu^\mu - \frac{2}{3}\Lambda g_\mu^\nu = 0$ , we obtain an elliptic equation for each metric component. Respective equations are given from  $\mathcal{G}_t^t$ ,  $(\mathcal{G}_t^t - \mathcal{G}_\rho^\rho - \mathcal{G}_\xi^\xi + 2\mathcal{G}_\theta^\theta)$  and  $\mathcal{G}_\theta^\theta$  as

$$\begin{aligned} \Delta T &= -\frac{4T}{z^2} \left( 1 + \frac{\Lambda\ell^2}{6} e^{2R} \right) - \frac{4\chi T_{,\xi}}{\rho^2} \left( \cot \chi + \frac{2r}{z} + 2\chi C_{,\xi} \right) + 2T_{,\rho} \left( \frac{1}{\rho} - \frac{2\ell}{\rho z} - C_{,\rho} \right) \\ &\quad + \frac{2T}{\rho} \left[ \left( 1 - \frac{\ell}{z} \right) C_{,\rho} - \frac{2\chi \sin \chi}{z} C_{,\xi} \right], \end{aligned} \quad (6)$$

$$\begin{aligned} \Delta R &= \frac{2}{z^2} \left( 1 + \frac{\Lambda\ell^2}{6} e^{2R} \right) + \frac{1 - e^{2(R-C)}}{r^2} + \frac{4\chi T_{,\xi}}{\rho^2 T} \left( \cot \chi + \frac{r}{z} + 2\chi C_{,\xi} \right) + \frac{2T_{,\rho}}{T} \left( \frac{\ell}{\rho z} + C_{,\rho} \right) \\ &\quad + \frac{4\chi C_{,\xi}}{\rho^2} \left( \cot \chi + \frac{2r}{z} + \chi C_{,\xi} \right) + C_{,\rho} \left( -\frac{2}{\rho} + \frac{4\ell}{\rho z} + C_{,\rho} \right), \end{aligned} \quad (7)$$

$$\begin{aligned} \Delta C &= -\frac{4}{z^2} \left( 1 + \frac{\Lambda\ell^2}{6} e^{2R} \right) - \frac{1 - e^{2(R-C)}}{r^2} - \frac{2\chi T_{,\xi}}{\rho^2 T} \left( \cot \chi + \frac{r}{z} + 2\chi C_{,\xi} \right) - \frac{T_{,\rho}}{T} \left( \frac{\ell}{\rho z} + C_{,\rho} \right) \\ &\quad - \frac{2\chi C_{,\xi}}{\rho^2} \left( 4 \cot \chi + \frac{5r}{z} + 4\chi C_{,\xi} \right) + C_{,\rho} \left( \frac{1}{\rho} - \frac{5\ell}{\rho z} - 2C_{,\rho} \right), \end{aligned} \quad (8)$$

where a comma means a partial derivative, and  $\Delta = \partial_r^2 + \partial_z^2 = \partial_\rho^2 + \rho^{-1}\partial_\rho + 2\rho^{-2}(2\xi\partial_\xi^2 + \partial_\xi)$  is the Laplace operator. The elliptic equations for  $R$  and  $C$  contain singular terms that behave as  $r^{-2} \propto \chi^{-2}$  when  $\chi \rightarrow 0$ . Introduction of  $\xi$  changes this severe behavior and it makes the terms more tractable in numerical calculation. Constraint equations are obtained, respectively, from  $\mathcal{G}_\xi^\rho$  and  $(\mathcal{G}_t^t - \mathcal{G}_\rho^\rho + \mathcal{G}_\xi^\xi + 2\mathcal{G}_\theta^\theta)$  as

$$\Theta_1 := \xi T \left( \frac{\ell^2 e^{2R}}{z^2} \right) \mathcal{G}_\xi^\rho,$$

$$\begin{aligned}
&= \xi \left[ R_{,\xi} T_{,\rho} - T_{,\xi\rho} + T_{,\xi} \left( R_{,\rho} + \frac{1}{\rho} \right) \right] + T \left[ \xi R_{,\xi} \left( 2C_{,\rho} - \frac{1}{\rho} + \frac{3\ell}{\rho z} \right) - 2\xi C_{,\xi\rho} - C_{,\rho} \left( \frac{\chi}{\tan \chi} + 2\xi C_{,\xi} \right) \right. \\
&\quad \left. + R_{,\rho} \left( \frac{\chi}{\tan \chi} + \frac{3r\sqrt{\xi}}{2z} + 2\xi C_{,\xi} \right) \right] = 0, \tag{9}
\end{aligned}$$

$$\begin{aligned}
\Theta_2 &:= -\frac{1}{2} \left( \frac{\ell^2 e^{2R}}{z^2} \right) \left( \mathcal{G}_t^t - \mathcal{G}_\rho^\rho + \mathcal{G}_\xi^\xi + 2\mathcal{G}_\theta^\theta \right), \\
&= \frac{4\xi T_{,\xi\xi}}{\rho^2} + \frac{2T_{,\xi}}{\rho^2} \left( 1 + \frac{2\chi}{\tan \chi} + \frac{3r\sqrt{\xi}}{z} + 2\xi(2C_{,\xi} - R_{,\xi}) \right) + T_{,\rho} \left( \frac{3\ell}{\rho z} + 2C_{,\rho} + R_{,\rho} \right) \\
&\quad + T \left[ \frac{6}{z^2} \left( 1 - \frac{|\Lambda|\ell^2}{6} e^{2R} \right) + \frac{1 - e^{2(R-C)}}{r^2} + \frac{8\xi C_{,\xi\xi}}{\rho^2} + \frac{12C_{,\xi}}{\rho^2} \left( \frac{1}{3} + \frac{\chi}{\tan \chi} + \frac{r\sqrt{\xi}}{z} + \xi C_{,\xi} \right) \right. \\
&\quad \left. + C_{,\rho} \left( \frac{6\ell}{\rho z} - \frac{2}{\rho} + C_{,\rho} \right) - \frac{2R_{,\xi}}{\rho^2} \left( \frac{2\chi}{\tan \chi} + \frac{3r\sqrt{\xi}}{z} + 4\xi C_{,\xi} \right) + R_{,\rho} \left( \frac{3\ell}{\rho z} - \frac{1}{\rho} + 2C_{,\rho} \right) \right] = 0. \tag{10}
\end{aligned}$$

We perform numerical calculations for the elliptic equations using a relaxation method. The constraint equations are not explicitly solved but they are used as a check of accuracy. Before proceeding further, we discuss an important property of the constraint equations [44]. The constraint equations multiplied some functions satisfy Cauchy-Riemann relations. They are obtained from the non-trivial components of the Bianchi identities  $\nabla_\mu \mathcal{G}^\mu_\nu = 0$ . Assuming that equations for  $T$ ,  $R$ , and  $C$  are satisfied, i.e.,  $\mathcal{G}_t^t = \mathcal{G}_\theta^\theta = (\mathcal{G}_\rho^\rho + \mathcal{G}_\xi^\xi) = 0$ , we obtain Cauchy-Riemann relations for  $\mathcal{G}_\xi^\rho$  and  $(\mathcal{G}_\rho^\rho - \mathcal{G}_\xi^\xi)$  as

$$\begin{aligned}
\partial_\xi \mathcal{U} - \partial_\chi \mathcal{V} &= 0, \\
\partial_\chi \mathcal{U} + \partial_\xi \mathcal{V} &= 0, \tag{11}
\end{aligned}$$

where  $\mathcal{U} := \xi \sqrt{-g} \mathcal{G}_\xi^\rho / \sin \theta$ ,  $\mathcal{V} := \rho \sqrt{-g} \sqrt{\xi} (\mathcal{G}_\rho^\rho - \mathcal{G}_\xi^\xi) / (4 \sin \theta)$  and  $g := \det(g_{\mu\nu})$ . Then

$$\begin{aligned}
\mathcal{U} &= \left( \frac{\ell}{z} \right)^3 \frac{\rho^3 e^{2C} (\sin \sqrt{\xi})^2}{2\sqrt{\xi}} \Theta_1, \\
\mathcal{V} &= \left( \frac{\ell}{z} \right)^3 \frac{\rho^4 e^{2C} (\sin \sqrt{\xi})^2}{4} \Theta_2. \tag{12}
\end{aligned}$$

Since  $\mathcal{U}$  and  $\mathcal{V}$  satisfy Cauchy-Riemann relations, each of them satisfies Laplace equation. Hence in principle, if  $\Theta_1 = 0$  is satisfied on all boundaries and provided that  $\Theta_2$  vanishes at any one point, the two constraint equations must be solved in all places as long as the elliptic equations for  $T$ ,  $R$ , and  $C$  are satisfied.

### C. Boundary conditions

In order to solve the elliptic equations derived in the previous section, we must specify the boundary conditions. Let us first discuss boundary conditions on the symmetry axis of  $r = 0$ . The regularity at  $r = 0$  of Eqs. (7) and (8) requires

$$R = C \quad (\text{at } \xi = 0), \tag{13}$$

which determines the boundary condition for  $R$ . The axial symmetry requires that  $r$  derivative of the metric functions vanishes at  $r = 0$ . However, as long as we use  $\xi$  coordinate, finiteness of the derivative in this coordinate automatically guarantees the regularity because  $T_{,r} \propto \sqrt{\xi} T_{,\xi}$ . Hence, we adopt a free boundary condition for  $T$  and  $C$ . The values of  $T$  and  $C$  at  $r = 0$  are evolved in the same way as the values at an ordinary grid point. The only difference is to use the one-sided differentiation to evaluate the first order derivatives with respect to  $\xi$ . The second order derivatives disappear at  $\xi = 0$  from the Laplace operator. Equation (9) at  $\xi = 0$  is trivial from Eq. (13), while Eq. (10) reduces to

$$R_{,\xi} = 3C_{,\xi} + \frac{T_{,\xi}}{T} + \rho^2 \left[ \frac{1 - e^{2R}}{z^2} + C_{,\rho} \left( \frac{2\ell - \rho}{2\rho z} + \frac{C_{,\rho}}{2} \right) + \frac{T_{,\rho}}{2T} \left( \frac{\ell}{\rho z} + C_{,\rho} \right) \right] \quad (\text{at } \xi = 0). \tag{14}$$

We can also show that this equation is guaranteed to be satisfied if  $R$  and  $C$  are solutions of Eqs. (7) and (8). Although it is not necessary in principle, we use this condition (14) in addition to Eq. (13) in order to improve the accuracy

of calculation. We do not solve the evolution equation for  $R$  at the ordinary grid points next to the axis in place of imposing this supplementary condition.

On the horizon, the Killing vector  $\partial_t$  must become null. Therefore we have

$$T = 0 \quad (\text{at } \rho = \rho_h), \quad (15)$$

In the present gauge, the horizon is given by a constant radius, and thus we have

$$T_{,\xi} = T_{,\xi\xi} = 0 \quad (\text{at } \rho = \rho_h), \quad (16)$$

Here we assume that metric functions and their derivatives are finite on the horizon. With the aid of Eqs. (15) and (16), the surface gravity on the horizon is given as

$$\kappa = e^{-R} T_{,\rho} \quad (\text{at } \rho = \rho_h). \quad (17)$$

This condition can be used to impose a Dirichlet boundary condition for  $R$  on the horizon. For this purpose, we rewrite it as

$$R = C|_{\xi=0} + \log\left(\frac{T_{,\rho}}{T_{,\rho}|_{\xi=0}}\right) \quad (\text{at } \rho = \rho_h), \quad (18)$$

using Eq. (13).

We can show, following the line of a standard proof [47], that the zeroth law of black hole thermodynamics that the surface gravity is constant on the horizon,  $\partial_\chi \kappa = 0$ , and it guarantees Eq. (9) to be satisfied on the horizon. Assuming the surface gravity is nonzero (non-extremal), we find that  $T_{,\rho}$  must be nonzero on the horizon;  $T_{,\rho} \neq 0$ . Then, from the regularity of Eq. (7) or Eq. (8) on the horizon, a condition for  $C_{,\rho}$  is derived as

$$C_{,\rho} = -\frac{\ell}{\rho_h z} \quad (\text{at } \rho = \rho_h). \quad (19)$$

On the other hand, the condition that the expansion is zero on the horizon gives [46]

$$(R + 2C)_{,\rho} + \frac{3\ell}{\rho_h z} = 0 \quad (\text{at } \rho = \rho_h), \quad (20)$$

which guarantees the constraint equation (10) on the horizon. In the following numerical calculation, we basically impose these Neumann boundary conditions on the horizon for  $R$  and  $C$ . As a supplementary condition to improve the accuracy, we also use Eq. (18), but we do not use Eq. (17). Hence, in our calculation the surface gravity is not given by hand as a parameter. We discuss this point in more detail at the end of this subsection.

For the extremal case  $\kappa = 0$ , the boundary conditions are not fully determined in the present way. From  $\kappa = 0$ ,  $R = \infty$  or  $T_{,\rho} = 0$  are required on the horizon, and thus the boundary condition for  $C$  are not determined from the regularity on the horizon. It might be interesting to explore the extremal case separately, but we do not consider it in this paper.

The Israel's junction condition for the RS braneworld model gives  $K_{\mu\nu} = -\gamma_{\mu\nu}/\ell$ , where  $\gamma_{\mu\nu}$  and  $K_{\mu\nu}$  are induced metric and extrinsic curvature on the brane, respectively. From this condition, we obtain the boundary conditions on the brane as

$$\frac{\partial_\xi T}{T} = \partial_\xi R = \partial_\xi C = -\frac{\rho}{2\ell\sqrt{\xi}} (1 - e^R) \quad (\text{at } \xi = (\pi/2)^2). \quad (21)$$

Constraint equation (9) is manifestly satisfied under these conditions.

We must also specify asymptotic boundary conditions. For the asymptotic infinity, the boundary conditions to obtain asymptotically AdS spacetime are  $T \rightarrow 1$  and  $R, C \rightarrow 0$ . The metric functions must smoothly approach these asymptotic values. In actual numerical calculations, these asymptotic boundary conditions are imposed at a finite, but sufficiently far region, and we must check that the solutions are insensitive to the position.

With these boundary conditions, we can solve the elliptic equations as a boundary value problem. Moreover, these boundary conditions guarantee the constraint equation  $\Theta_1$  to be satisfied on all boundaries and  $\Theta_2$  to be satisfied at least on the horizon. Hence the two constraint equations are automatically satisfied as long as the elliptic equations are exactly solved.

It should be noted that all elliptic equations, constraint equations and boundary conditions can be rewritten in terms of non-dimensional coordinates  $\{\hat{\rho}, \chi\}$ , where  $\hat{\rho} := \rho/\ell$ , without any dimensionful parameters. Then this system of equations, and hence a black hole solution is characterized only by a single parameter

$$L = \ell/\rho_h. \quad (22)$$

In our numerical calculation, we take  $\rho_h \equiv 1$  and change  $\ell$  to specify this parameter, since we want to fix a coordinate region where numerical calculations are performed. The variation of  $\ell$  keeping  $L$  fixed corresponds to a rescale of the length scale as we notice from the metric (1), which is rewritten as

$$ds^2 = \ell^2 ds_L^2(\hat{t}, \hat{\rho}, \chi), \quad (23)$$

where  $ds_L^2$  is non-dimensional part of the line element written by  $\{\hat{t} = t/\ell, \hat{\rho}, \chi\}$ , and its metric function is given by a black hole solution  $T, R$  and  $C$  with the parameter  $L$ . After specifying a black hole solution by this method, one may want to transform the solutions to those in the coordinates where  $L$  is specified by taking  $\ell \equiv 1$  and changing  $\rho_h$ . For this purpose, it is enough to multiply  $\ell^{-1}$  to a length scale in the coordinates where  $\rho_h \equiv 1$  is taken.

A question may arise. Although we say that we use

$L = \ell/\rho_h$  to specify a solution,  $\rho_h$  does not have a clear physical meaning. One may think that it is more appropriate to specify the value of the surface gravity  $\kappa$  instead of  $\rho_h$ . Here we should recall the argument given at the end of the preceding subsection that  $\rho/\rho_h$  and hence  $\hat{\rho}/\hat{\rho}_h$  cannot be changed arbitrarily by using the residual gauge degrees of freedom. If we change the value of  $\hat{\rho}_h$  by using this residual gauge degrees of freedom, the value of  $\hat{\rho}$  at infinity also scales correspondingly. Then, we will see that the asymptotic boundary conditions  $T \rightarrow 1$  and  $R, C \rightarrow 0$  are not satisfied after the gauge transformation. Hence, for a given solution we do not have a degree of freedom to change the value of  $\hat{\rho}_h$  arbitrarily. Thus, if we specify a solution by fixing both  $\kappa$  and  $\ell$ , we are not allowed to set  $\rho_h = 1$  any further. To the contrary, as we wish to set  $\rho_h = 1$  in the actual numerical computation, we should not use the condition (17) that specifies the value of  $\kappa$  directly.

### III. NUMERICAL SOLUTIONS OF SMALL BLACK HOLES

#### A. Comparison with 5D Schwarzschild solution

The formulation outlined in the previous section indeed works well to solve the Einstein equations as a boundary value problem, using an iterative convergence scheme of relaxation method. A simple check of an algorithm is to calculate very large limit of  $L$  for fixed  $\rho_h$ , and compare the result with the 5D Schwarzschild solution in isotropic coordinates which is the solution in the flat background limit  $\ell \rightarrow \infty$  taking  $z/\ell \rightarrow 1$ ;

$$\begin{aligned} T(\rho) &= \frac{\rho^2 - \rho_h^2}{\rho^2 + \rho_h^2}. \\ R(\rho) &= C(\rho) = \log \left( 1 + \frac{\rho_h^2}{\rho^2} \right). \end{aligned} \quad (24)$$

We have used this solution as an initial guess configuration with which we start the relaxation. Namely, we first calculated a solution for relatively large  $L$ , and then proceeded to smaller  $L$  by using the result relaxed for the previous value of  $L$  as an initial configuration. In this paper we restrict the numerical calculations only to small black holes that are characterized by  $L > 1$ . This limitation is due to a practical reason that it is difficult to converge the numerical calculations with sufficiently small numerical errors for  $L \lesssim 1$ .

To orient the reader, we show a result of  $T, R$ , and  $C$  for  $L = 15$  in Figure 1 as a typical example. The center of the black hole is at  $r = 0$  and  $z - \ell = 0$ . Interior of the horizon  $\rho < \rho_h$  is outside the region of our numerical calculation. The contours of  $T$  is almost spherical for this value of  $L$  as in the case of the limit  $L \rightarrow \infty$  in spite of the non-trivial boundary conditions on the brane, while the contours of  $R$  and  $C$  manifestly deviate from spherical shape.

In Figure 2, the solution for  $L = 30$  is displayed in the polar coordinates that are more appropriate to see the angular dependence of the metric functions. Figure 3 displays the results for  $L = 10$  in the polar coordinates. The deviations from spherical shape for  $L = 10$  are enhanced more than those for  $L = 30$ . We have performed numerical calculations for the parameter region  $L = 3 \sim 500$ . The results for some  $L$  are listed in Table I.

The constraint equations for each numerical solution show that the absolute errors of the constraint equations,  $|\Theta_1|$  and  $|\Theta_2|$ , are observed mainly around the origin of polar coordinates and near the horizon (Figure 4), where the elliptic equations have the terms whose coefficients behave like  $1/\xi \rightarrow \infty$  or  $1/T \rightarrow \infty$ . These violations of the constraint equations are general features of the present calculations and they become larger as  $L$  becomes smaller. Averaged violations of the equations are listed in Table I. In the table and its caption, we have introduced a norm  $N(\xi, \rho)$  of the constraint equations, to obtain relative accuracies of the constraint equations,  $|\Theta_1|/N_1$  and  $|\Theta_2|/N_1$ . Figure 4 shows that the relative accuracy around the horizon is not so bad, although the absolute errors are significant there. On the other hand, the figure represents that the relative accuracy becomes worse near the axis. The lack of accuracy near the axis is a common problem in axisymmetric problems. The number of grid points  $(\xi_i, \rho_j)$  used in our calculation

is  $100 \times 1000$ . The grid point  $\rho_j$  is taken to be a geometric progression  $\rho_j = \rho_h + \epsilon(1 - \gamma^j)/(1 - \gamma)$ . The parameters  $\epsilon$  and  $\gamma$  are determined by requiring that the ratio of the last grid resolution to the first one is  $\delta\rho_{\max}/\delta\rho_1 \approx 2.71$  and the asymptotic boundary is set at  $\rho_{\max} = 85$ . It is crucial to test the sensitivity of the solutions to the physical size of the lattice. This is discussed at the end of the next section.

Convergences of numerical calculation become worse as  $L$  becomes smaller, and errors of constraint equations also grow. This is observed from the averaged error of each calculation (see Table I for details). It becomes in general more difficult to find solutions as the nonlinear effects of differential equations grow. We could not keep sufficient accuracy to construct large black holes ( $L \lesssim 1$ ) so that the calculation breaks down in the end. Thus in this paper we concentrate only on small black holes ( $L > 1$ ), although it is important to improve our scheme by identifying and removing the ultimate origin of numerical instabilities.

### B. Thermodynamic quantities

We are more interested in the deviations of the numerically obtained solutions from the 5D Schwarzschild solution. To quantify the deviations, we focus on thermodynamic quantities. The surface gravity (or temperature) is determined by Eq. (17), and the area (or entropy) of a black hole horizon is given by

$$A_5 = 2\rho_h^3 \int d\Omega \int_0^{(\pi/2)^2} d\xi \frac{\sin^2 \sqrt{\xi}}{2\sqrt{\xi}} \left(\frac{\ell}{z}\right)^3 e^{R+2C}. \quad (25)$$

Here the factor 2 is due to  $Z_2$  symmetry. The proper area of the intersection between the horizon and the brane is given by

$$A_4 = 4\pi\rho_h^2 e^{2C} \quad (\chi = \pi/2). \quad (26)$$

For comparison we quote the corresponding thermodynamic quantities for the 5D Schwarzschild-AdS (SA) solution and the black string (BS);

$$\begin{aligned} \kappa_{\text{SA}} &= \frac{1}{\varpi} + \frac{2\varpi}{\ell^2}, \\ A_{5\text{SA}} &= 2\pi^2\varpi^3, \\ A_{4\text{SA}} &= 4\pi\varpi^2, \end{aligned} \quad (27)$$

and

$$\begin{aligned} \kappa_{\text{BS}} &= \frac{1}{2\varpi}, \\ A_{5\text{BS}} &= 4\pi\varpi^2\ell, \\ A_{4\text{BS}} &= 4\pi\varpi^2. \end{aligned} \quad (28)$$

Here  $\varpi$  is the circumferential radius of horizon. These thermodynamic quantities have been evaluated for our numerical solutions. As we have explained before, there is a degree of freedom of changing the overall length scale, and hence, for comparison, we have to use non-dimensional combination of the thermodynamic quantities. Notice that  $\rho_h$  in our numerical calculation does not have a clear geometrical meaning, and it is not a relevant quantity to make a non-dimensional combination.

In Figures 5 and 6 we show the behavior of the relations between thermodynamic quantities. Figure 5 gives a relation between the 4D area  $A_4$  and the surface gravity  $\kappa$  taking an appropriate non-dimensional combination. In the figure the thermodynamic relations for the 4D and the 5D Schwarzschild solutions are also plotted for comparison. We observe that for large  $L$ , i.e., for very small black holes, the numerical solutions behave like the 5D Schwarzschild solution, and then as  $L$  becomes small they deviate from the 5D Schwarzschild black hole and show a tendency to behave like the 4D Schwarzschild black hole. Figure 6 shows the same tendency by using a relation between the 5D area and the surface gravity. When the horizon is sufficiently small ( $\kappa\ell \gg 1$ ), the result for the numerical solutions approximately coincide with the line expected by the 5D Schwarzschild-AdS solution. However, as the horizon radius increases, the plot points for the numerical solutions deviate from it, toward the opposite direction. In the end they cross the line for the black string.

Mass of black hole is one of important quantities of black hole. We can calculate thermodynamic mass from the first law of thermodynamics  $dM = (\kappa/8\pi)dA$ . In order to integrate the first law, we interpolated the thermodynamical quantities obtained for discrete values of  $L$  up to  $L = 5$ . The smallest numerically obtained black hole ( $L = 500$ ) was smoothly extrapolated to the 5D Schwarzschild black hole. Figure 7 shows the mass-entropy relation. For

comparison, the mass-entropy relations for the black string and the 5D Schwarzschild solution are also plotted. We see that the entropy of the localized black hole ( $L \gtrsim 5$ ) is greater than that of the other references with the same mass. Extrapolating the curves, however, one notices that the entropy of the black string is likely to get larger than that of the localized black hole as the mass increases. If so, the localized black hole solution seems to be unstable from the viewpoint of the entropy. Of course, as we know that the black string is dynamically unstable irrespective of the mass, the larger entropy does not mean the dynamical stability of the black string [10]. This observation might be very suggestive, but we cannot provide any conclusive statement about the dynamical stability of the localized black hole because the stability based on entropy does not directly indicate the dynamical stability.

We can compare the thermodynamic relation of the 5D localized black hole with the relation of the EHM solution in the 4D braneworld (Figure 8) [29]. One can see a similar behavior of thermodynamic relation for  $\ln \kappa \ell \gtrsim 0$ , and it seems to give an insight toward extrapolating the thermodynamic relation to larger black hole solutions. However, there is a big difference between the 5D model and the 4D model as discussed in Refs. [33, 34]. On one hand, in the case of the 5D model the metric induced on the brane for a large black hole is expected to mimic the 4D Schwarzschild metric with some small corrections. On the other hand, 3D black hole solution that corresponds to the 4D Schwarzschild metric in the 5D model does not exist. Thus we cannot naively apply the analogy of the EHM solution. Furthermore, the numerical errors of the solutions also grow along the flow of the solutions. We could not obtain sufficiently relaxed numerical solutions for  $L \lesssim 1$ . Hence, at present we cannot say anything definite for large black hole solutions.

Let us consider the shape of the small localized black hole in the bulk. Figure 9 shows the ratio of a mean radius in four-dimension  $A_4^{1/2}$  (on the brane) to that in five-dimension  $A_5^{1/3}$ . The figure indicates that the black hole tends to flatten as its horizon radius increases. This behavior is expected from the AdS geometry of whole spacetimes. The so-called warp factor  $\ell z^{-1}$  of the AdS geometry (1) will in general make the localized black hole to be flattened, and this effect becomes significant when the horizon radius is large. In fact, the EHM solution exhibits a flattened geometry [29].

Before concluding this section, we give comments on checks of our numerical calculations. We have checked second order convergences of the thermodynamic quantities for  $L = 20$  keeping  $\rho_{\max} = 85$ . As a function of  $\delta \xi$ , we confirmed the quadratic fits for  $\kappa$  and  $A_5$ . The similar quadratic fit is possible for the variation of  $\rho$  resolution, in which we need to change the lattice resolution keeping the ratio  $\delta \rho_{\max}/\delta \rho_1$  fixed ( $\approx 2.71$ ). The numbers of grid points  $(\xi_i, \rho_j)$  used in these checks are  $(80 \sim 200) \times 1000$  for  $\delta \xi$  variation, and  $100 \times (750 \sim 2000)$  for  $\delta \rho$  variation, which correspond to  $\delta \xi = 0.01 \sim 0.03$  and  $\delta \rho = 0.02 \sim 0.07$ , respectively. As for the absolute errors of constraint equations,  $|\Theta_1|$  and  $|\Theta_2|$ , it is observed that the absolute errors decrease as the lattice resolutions increase. However clear second order convergences have not observed because of the geometric progression of grid point  $\rho_j$ . If we use equal grid spacings, second order convergences are observed. We have also checked the insensitivity of our numerical solutions on the finite position of the asymptotic boundary. To confirm it, we vary the position  $\rho_{\max}$  for  $L = 10$  and  $L = 20$ , and check the robustness of thermodynamic quantities. For each variation of  $\rho_{\max}$ , we have changed the grid resolution for  $\rho$  keeping the ratio  $\delta \rho_{\max}/\delta \rho_1 \approx 2.71$  with  $\delta \rho_1 \approx 0.05$ . The thermodynamic quantities are stable for each value of  $\rho_{\max}$ , and then the thermodynamic relations are also stable. Figure 10 shows a result. One sees that the non-dimensional combination of thermodynamic quantities is stable and the variation is no more than 1% for the parameters.

#### IV. DISCUSSION

Black hole solutions that represent a black hole localized on the brane in Randall-Sundrum infinite braneworld model have not been found in appropriate boundary conditions. We have explored this problem in this paper. We have performed the numerical calculations and found non-trivial localized black hole solutions whose horizon radii  $\rho_h$  are small compared to the bulk curvature scale  $\ell$ . More precisely, *the small localized black hole solutions are approximately constructed by numerical calculations under appropriate boundary conditions*. We could not succeed in finding black hole solutions with large horizon radius. The convergence of the relaxation method becomes slower for larger horizon radius, and we could not keep enough accuracy of computation in the end.

In the limit of small black hole,  $\ell/\rho_h \rightarrow \infty$ , the 5D Schwarzschild black hole is the solution. Then we are interested in the deviations of the small localized black holes from the 5D Schwarzschild black hole. To observe it by quantitative comparison, the thermodynamic quantities are calculated for these small black holes. We found that the numerically obtained solutions significantly deviate from the naive expectation based on the 5D Schwarzschild-AdS solution as its horizon radius increases (Figure 6). The comparison of the thermodynamic quantities also suggests that the numerical solutions approach to solutions whose induced metric on the brane behaves like the 4D Schwarzschild solution (Figure 5), although we could not obtain a clear evidence for it from the direct comparison of the induced metric. Moreover, we could observe the transition of the shape of the small localized black hole in the bulk (Figure 9). The black hole tends to flatten as its horizon radius increases. This is expected due to the nature of the AdS geometry, and is also observed

in the EHM solution of localized black hole in the 4D braneworld [29]. Although the EHM solution is the solution in the lower dimensions, it is interesting to compare our solution with it. We have compared the thermodynamic relation of the EHM solution with that of the 5D numerical solutions, and observed a similarity between them (Figure 8). This observation might be suggestive, but since our calculations are restricted only to small black hole solutions ( $\rho_h/\ell < 1$ ), we could not discuss anything definite about large black hole solutions ( $\rho_h/\ell \gtrsim 1$ ). Thus, it is an important open question to identify the character of large black hole solutions. In particular, the induced gravity and its deviation from the 4D Schwarzschild black hole at large distance are interesting. It may be worth pointing out that since we do not have any uniqueness theorem in the context of the braneworld [48, 49], there is a possibility of finding another sequence of solutions than that found in this paper if we start with a completely different initial guess.

Here we discuss the relation between our results and the classical black hole evaporation conjecture [33, 34]. Based on the AdS/CFT correspondence, it was argued that there might be no static black hole solution in the Randall-Sundrum single brane model. One might think that the fact that we have numerically found small black hole solutions conflicts with this conjecture. However, there are two possible consistent scenarios. One is that only small black hole solutions are admitted to exist. Since the classical evaporation conjecture applies only for sufficiently large black holes, for which the quantum correction in the AdS picture is negligible, the existence of small black hole solutions does not directly conflict with the conjecture. However, the relations between thermodynamic quantities anticipate that there is no critical point at which the sequence of solutions suddenly terminates to exist. Therefore, we think that this first possibility is less likely. The other possibility is that even small black hole solutions are allowed only in an approximate sense. Even if there is no black hole solution in a strict sense irrespective of its size, the internal inconsistency contained in the setup of the problem might be absorbed by numerical errors. If this is the case, the failure of finding larger black hole solutions might be a signal of increase of the inconsistency. Of course, there also remains the possibility that the classical evaporation conjecture turns out to be incorrect. Unfortunately, however, we cannot say anything definite about these points at the moment because the lack of convergence in the relaxation scheme that we encountered can be purely technical issue of numerical method. For example, an unstable mode that appears near the axis is a common problem in axisymmetric code.

As a direction of future work, it is crucially important to find large black hole solutions if they exist, and it needs further developments of technique and investigation. It is also interesting to apply this method to find the black holes localized on the TeV brane [4]. The stabilities of higher dimensional black hole including our solution are also important. A part of the works is in progress and it will appear in our future publication. We wish the method used in this paper will become a basis of the further studies on black holes in higher dimensions.

### Acknowledgments

We would like to thank Shu-ichiro Inutsuka, Toby Wiseman, Tetsuya Shiromizu, Roberto Emparan, Nemanja Kaloper and Shinji Mukohyama for their helpful comments and suggestions. To complete this work, the discussion during and after the YITP workshops YITP-W-01-15 and YITP-W-02-19 were useful. Numerical computations in this work were carried out at the Yukawa Institute Computer Facility. H.K. is supported by JSPS Research Fellowships for Young Scientists. This work is partly supported by the Monbukagakusho Grant-in-Aid No. 1270154.

---

[1] N. Arkani-Hamed, S. Dimopoulos and G. R. Dvali, “The hierarchy problem and new dimensions at a millimeter,” *Phys. Lett. B* **429**, 263 (1998); I. Antoniadis, N. Arkani-Hamed, S. Dimopoulos and G. R. Dvali, “New dimensions at a millimeter to a Fermi and superstrings at a TeV,” *Phys. Lett. B* **436**, 257 (1998)

[2] S. B. Giddings and S. Thomas, “High energy colliders as black hole factories: The end of short distance physics,” *Phys. Rev. D* **65**, 056010 (2002)

[3] S. Dimopoulos and G. Landsberg, “Black holes at the LHC,” *Phys. Rev. Lett.* **87**, 161602 (2001)

[4] L. Randall and R. Sundrum, “A large mass hierarchy from a small extra dimension,” *Phys. Rev. Lett.* **83**, 3370 (1999)

[5] L. Randall and R. Sundrum, “An alternative to compactification,” *Phys. Rev. Lett.* **83**, 4690 (1999)

[6] R. C. Myers and M. J. Perry, “Black Holes In Higher Dimensional Space-Times,” *Annals Phys.* **172**, 304 (1986).

[7] F.R. Tangherlini, *Nuovo Cimento* **27**, 636 (1963).

[8] R. C. Myers, “Higher Dimensional Black Holes In Compactified Space-Times,” *Phys. Rev. D* **35**, 455 (1987).

[9] A. R. Bogojevic and L. Perivolaropoulos, “Black Holes In A Periodic Universe,” *Mod. Phys. Lett. A* **6**, 369 (1991).

[10] R. Gregory and R. Laflamme, “Black strings and p-branes are unstable,” *Phys. Rev. Lett.* **70**, 2837 (1993), R. Gregory, “Black string instabilities in anti-de Sitter space,” *Class. Quant. Grav.* **17**, L125 (2000)

[11] T. Hirayama and G. Kang, “Stable black strings in anti-de Sitter space,” *Phys. Rev. D* **64**, 064010 (2001)

[12] N. Dadhich, R. Maartens, P. Papadopoulos and V. Rezania, “Black holes on the brane,” *Phys. Lett. B* **487**, 1 (2000)

[13] I. Giannakis and H. C. Ren, “Possible extensions of the 4-D Schwarzschild horizon in the brane world,” *Phys. Rev. D* **63**, 125017 (2001)

[14] A. Chamblin, H. S. Reall, H. A. Shinkai and T. Shiromizu, “Charged brane-world black holes,” *Phys. Rev. D* **63**, 064015 (2001)

[15] C. Cadeau and E. Woolgar, “New five dimensional black holes classified by horizon geometry, and a Bianchi VI braneworld,” *Class. Quant. Grav.* **18**, 527 (2001)

[16] S. I. Vacaru and E. Gaburov, “Anisotropic black holes in Einstein and brane gravity,” [hep-th/0108065](#).

[17] S. I. Vacaru, “A new method of constructing black hole solutions in Einstein and 5D gravity,” [hep-th/0110250](#).

[18] P. Kanti and K. Tamvakis, “Quest for localized 4-D black holes in brane worlds,” *Phys. Rev. D* **65**, 084010 (2002)

[19] R. Casadio, A. Fabbri and L. Mazzacurati, “New black holes in the brane-world?,” *Phys. Rev. D* **65**, 084040 (2002)

[20] R. Casadio and L. Mazzacurati, “Bulk shape of brane-world black holes,” [gr-qc/0205129](#).

[21] G. Kofinas, E. Papantonopoulos and V. Zamarias, “Black hole solutions in braneworlds with induced gravity,” [hep-th/0208207](#).

[22] G. Sengupta, “Rotating black holes in higher dimensional brane worlds,” [hep-th/0205087](#).

[23] M. S. Modgil, S. Panda and G. Sengupta, “Rotating brane world black holes,” *Mod. Phys. Lett. A* **17**, 1479 (2002)

[24] H. Kodama, “Vacuum branes in D-dimensional static spacetimes with spatial symmetry  $IO(D-2)$ ,  $O(D-1)$  or  $O+(D-2,1)$ ,” [gr-qc/0204042](#).

[25] A. Chamblin, S. W. Hawking and H. S. Reall, “Brane-world black holes,” *Phys. Rev. D* **61**, 065007 (2000).

[26] R. Emparan and H. S. Reall, “Generalized Weyl solutions,” *Phys. Rev. D* **65**, 084025 (2002)

[27] R. Emparan and H. S. Reall, “A rotating black ring in five dimensions,” *Phys. Rev. Lett.* **88**, 101101 (2002)

[28] For example, R. Emparan, R. Gregory and C. Santos, “Black holes on thick branes,” *Phys. Rev. D* **63**, 104022 (2001) Y. Morisawa, R. Yamazaki, D. Ida, A. Ishibashi and K. i. Nakao, “Thick domain walls intersecting a black hole,” *Phys. Rev. D* **62**, 084022 (2000)

[29] R. Emparan, G. T. Horowitz and R. C. Myers, “Exact description of black holes on branes,” *JHEP* **0001**, 007 (2000); “Exact description of black holes on branes. II: Comparison with BTZ black holes and black strings,” *JHEP* **0001**, 021 (2000)

[30] G. T. Horowitz and K. Maeda, “Fate of the black string instability,” *Phys. Rev. Lett.* **87**, 131301 (2001)

[31] T. Wiseman, “Static axisymmetric vacuum solutions and non-uniform black strings,” [hep-th/0209051](#); T. Wiseman, “From black strings to black holes,” [hep-th/0211028](#).

[32] M. Bruni, C. Germani and R. Maartens, “Gravitational collapse on the brane,” *Phys. Rev. Lett.* **87**, 231302 (2001)

[33] T. Tanaka, “Effective Gravity in Randall-Sundrum Infinite Brane World,” *Int. J. Theor. Phys.* **41**, 2287-2297 (2002); T. Tanaka, “Classical black hole evaporation in Randall-Sundrum infinite braneworld,” [gr-qc/0203082](#).

[34] R. Emparan, A. Fabbri and N. Kaloper, “Quantum black holes as holograms in AdS braneworlds,” *JHEP* **0208**, 043 (2002)

[35] T. Shiromizu, K. I. Maeda and M. Sasaki, “The Einstein equations on the 3-brane world,” *Phys. Rev. D* **62**, 024012 (2000); M. Sasaki, T. Shiromizu and K. I. Maeda, “Gravity, stability and energy conservation on the Randall-Sundrum brane-world,” *Phys. Rev. D* **62**, 024008 (2000)

[36] J. Garriga and T. Tanaka, “Gravity in the brane-world,” *Phys. Rev. Lett.* **84**, 2778 (2000)

[37] T. Tanaka and X. Montes, “Gravity in the brane-world for two-branes model with stabilized modulus,” *Nucl. Phys. B* **582**, 259 (2000)

[38] S. Mukohyama and L. Kofman, “Brane gravity at low energy,” *Phys. Rev. D* **65**, 124025 (2002)

[39] T. Tanaka, “Asymptotic behavior of perturbations in Randall-Sundrum brane-world,” *Prog. Theor. Phys.* **104**, 545 (2000)

[40] I. Giannakis and H. C. Ren, “Recovery of the Schwarzschild metric in theories with localized gravity beyond linear order,” *Phys. Rev. D* **63**, 024001 (2001)

[41] H. Kudoh and T. Tanaka, “Second order perturbations in the Randall-Sundrum infinite brane-world model,” *Phys. Rev. D* **64**, 084022 (2001)

$L$	$\langle  TRC  \rangle$	$\langle  \Theta_1  \rangle$	$\langle  \Theta_2  \rangle$	$(\langle N_1 \rangle, \langle N_2 \rangle)$	$\kappa$	$A_5$	$A_4$	
5	$5.9 \times 10^{-4}$	$6.8 \times 10^{-4}$	$6.8 \times 10^{-4}$	$(2.2 \times 10^{-2}, 3.7 \times 10^{-2})$	0.37	129	53	
10	$1.3 \times 10^{-4}$	$2.2 \times 10^{-4}$	$1.6 \times 10^{-4}$	$(1.2 \times 10^{-2}, 2.7 \times 10^{-2})$	0.41	150	53	
15	$9.7 \times 10^{-5}$	$2.5 \times 10^{-4}$	$1.4 \times 10^{-4}$	$(9.2 \times 10^{-3}, 2.5 \times 10^{-2})$	0.43	155	53	
30	$7.4 \times 10^{-5}$	$1.7 \times 10^{-4}$	$9.3 \times 10^{-5}$	$(5.8 \times 10^{-3}, 2.4 \times 10^{-2})$	0.46	161	52	
50	$6.3 \times 10^{-5}$	$1.2 \times 10^{-4}$	$6.2 \times 10^{-5}$	$(4.8 \times 10^{-3}, 2.4 \times 10^{-2})$	0.47	160	51	
100	$5.0 \times 10^{-5}$	$6.9 \times 10^{-5}$	$5.6 \times 10^{-5}$	$(4.1 \times 10^{-3}, 2.3 \times 10^{-2})$	0.48	158	51	
500	$9.8 \times 10^{-6}$	$1.4 \times 10^{-5}$	$1.7 \times 10^{-5}$	$(3.6 \times 10^{-3}, 2.3 \times 10^{-2})$	0.50	158	50	
$L = \infty$						0.50	158	50

TABLE I: Table summarizing the data of numerical calculations for several values of  $L = \ell/\rho_h$ . In the calculations we have varied  $\ell$  keeping the horizon radius  $\rho_h = 1$ . Thus it should be noted that the dimensionful parameters, i.e., surface gravity  $\kappa$ , 5D area  $A_5$  and 4D area  $A_4$ , must be rescaled for comparison as we have explained below Eq. (22). In the table,  $L = \infty$  represents the 5D Schwarzschild black hole, which is the exact solution in this limit. To match the circumstance used in Eq. (27) with that of Eq. (24) in the coordinates (1), we must take  $\varpi = 2$  in Eq. (27).  $\langle |\Theta_1| \rangle$ ,  $\langle |\Theta_2| \rangle$ , and  $\langle |TRC| \rangle$  are averaged violations of the constraint equations and the elliptic equations.  $\langle |TRC| \rangle$  is the mean absolute value for the equations of  $T$ ,  $R$  and  $C$  with equal weight for each grid point. In taking these averages, the first 5% of lattice points in  $\xi$  and the region near the horizon  $\rho < 2\rho_h$  are excluded since they receive large enhancements of errors due to singular terms. We need appropriate references to compare with the violations of constraint equations. For this purpose, defining  $N(\xi, \rho)$  by  $N(\xi, \rho) = \sum_k |n^{(k)}(\xi, \rho)|$  where  $n^{(k)}$  represents the terms in  $\Theta_1$  or  $\Theta_2$  at  $(\xi, \rho)$ , we introduce  $\langle N_1 \rangle$  and  $\langle N_2 \rangle$  as the averaged value of  $N$  for  $\Theta_1$  and  $\Theta_2$ , respectively, in the restricted grid region mentioned above. The comparison of this norm and the violation of constraint equation gives a degree of cancellation between different terms. We see that the averaged constraint violations against  $\langle N_1 \rangle$  and  $\langle N_2 \rangle$  are small, and thus the constraint equations appear to be satisfied with sufficient accuracy, although the accuracy decreases as  $L$  decreases. The surface gravity  $\kappa$ , the 5D area  $A_5$  and the 4D area  $A_4$  are calculated for each numerically obtained solution using Eqs. (17), (25) and (26). The number of grid points  $(\xi_i, \rho_j)$  used in the calculations presented in this paper is  $100 \times 1000$ . The coordinate position of grid point  $\rho_j$  is taken to be a geometric progression  $\rho_j = \rho_h + \epsilon(1 - \gamma^j)/(1 - \gamma)$ . The grid spaces used in the calculation are  $\delta\xi = 0.025$ ,  $\delta\rho_1 = 0.049$ ,  $\delta\rho_{\max}/\delta\rho_1 = 2.714$ . The position of the asymptotic boundary is set at  $\rho_{\max} = 85$ .

- [42] H. Kudoh and T. Tanaka, “Second order perturbations in the radius stabilized Randall-Sundrum two branes model,” Phys. Rev. D **65**, 104034 (2002)
- [43] H. Kudoh and T. Tanaka, “Second order perturbations in the radius stabilized Randall-Sundrum two branes model. II: Effect of relaxing strong coupling approximation,” hep-th/0205041.
- [44] T. Wiseman, “Relativistic stars in Randall-Sundrum gravity,” Phys. Rev. D **65**, 124007 (2002)
- [45] T. Nakamura, K. i. Maeda, S. Miyama and M. Sasaki, “General Relativistic Collapse of an Axially Symmetric Star. I,” Prog. Theor. Phys. **63**, 1229 (1980).
- [46] See for example, D. M. Eardley, “Black hole boundary conditions and coordinate conditions,” Phys. Rev. D **57**, 2299 (1998)
- [47] R. M. Wald, *General Relativity* (The University of Chicago Press, 1984)
- [48] G. W. Gibbons, D. Ida and T. Shiromizu, “Uniqueness of (dilatonic) charged black holes and black p-branes in higher dimensions,” Phys. Rev. D **66**, 044010 (2002)
- [49] G. W. Gibbons, D. Ida and T. Shiromizu, “Uniqueness and non-uniqueness of static black holes in higher dimensions,” Phys. Rev. Lett. **89**, 041101 (2002)

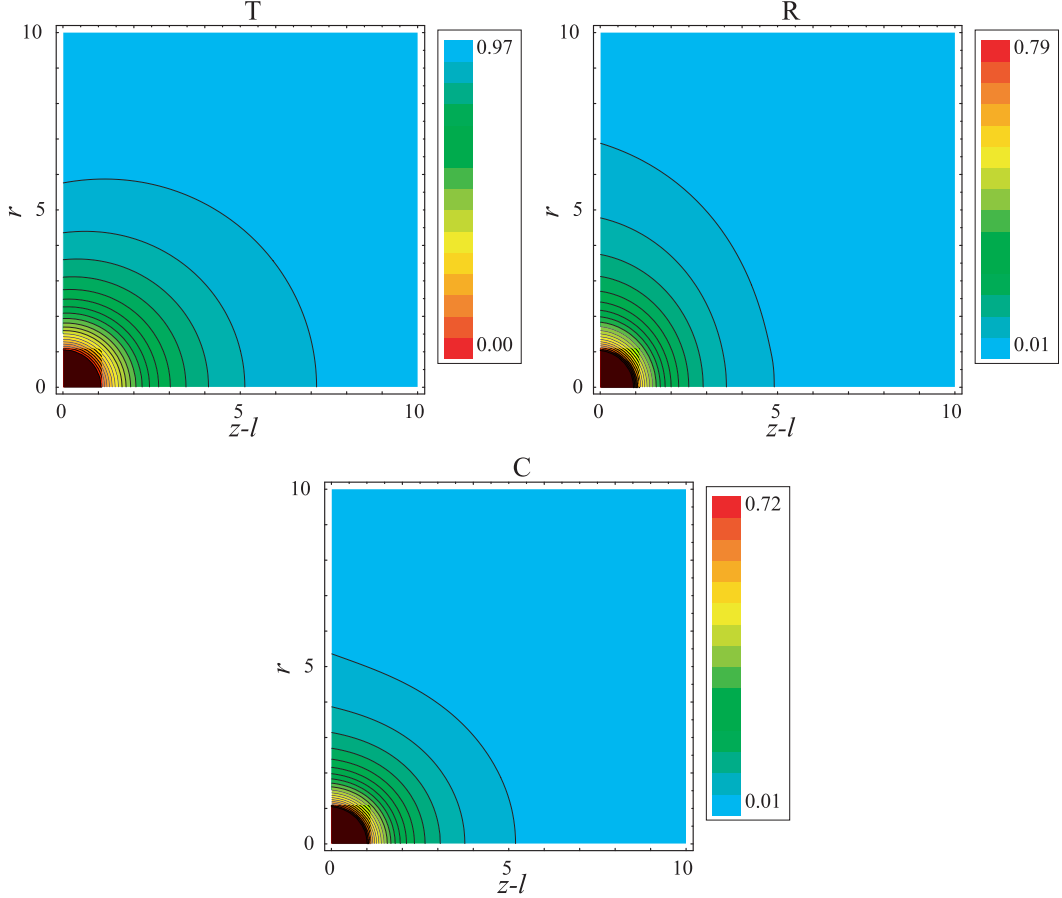


FIG. 1: An illustration of the metric functions  $T$ ,  $R$ , and  $C$  for  $L = 15$  in the coordinates  $\{r, z\}$ . This is a typical example of our numerical solutions for small black holes ( $L \gtrsim 5$ ). In these figures the center of the black hole is placed at the bottom left corner ( $r = 0$  and  $z - \ell = 0$ ), and the brane is at  $z - \ell = 0$ . The numerical calculation has been performed in the polar coordinates  $\{\rho, \xi\}$ , and hence the inner region of the black hole  $\rho < \rho_h$  is outside the area of our computation. Despite of the nontrivial boundary conditions at the brane, the contours of  $T$  is almost spherical in these coordinates even at far region from the horizon, which is fixed to be spherical by a conformal transformation. However, the contours for  $R$  and  $C$  deviate from the spherical shape at the far region.

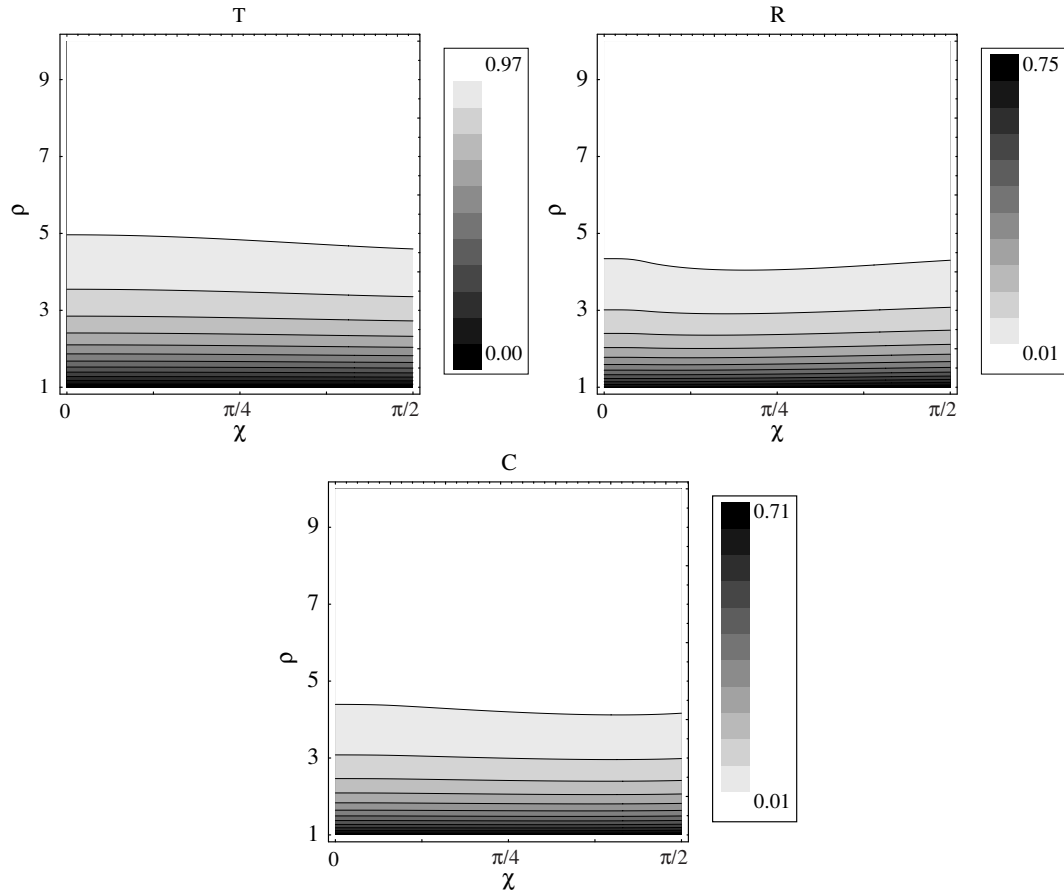


FIG. 2: An illustration of the solution for  $L = 30$  in polar coordinates  $\{\rho, \chi\}$ .

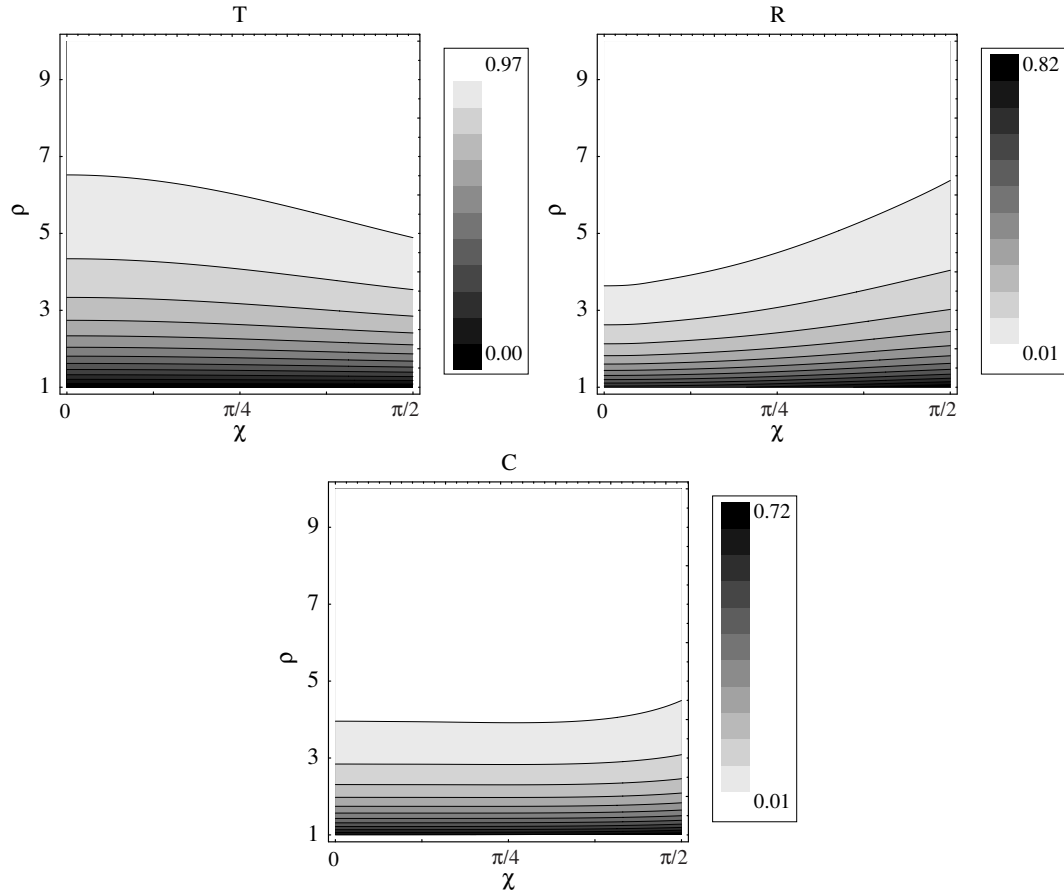


FIG. 3: An illustration of the metric functions  $T$ ,  $R$ , and  $C$  for  $L = 10$  in the coordinates  $\{\rho, \chi\}$ .

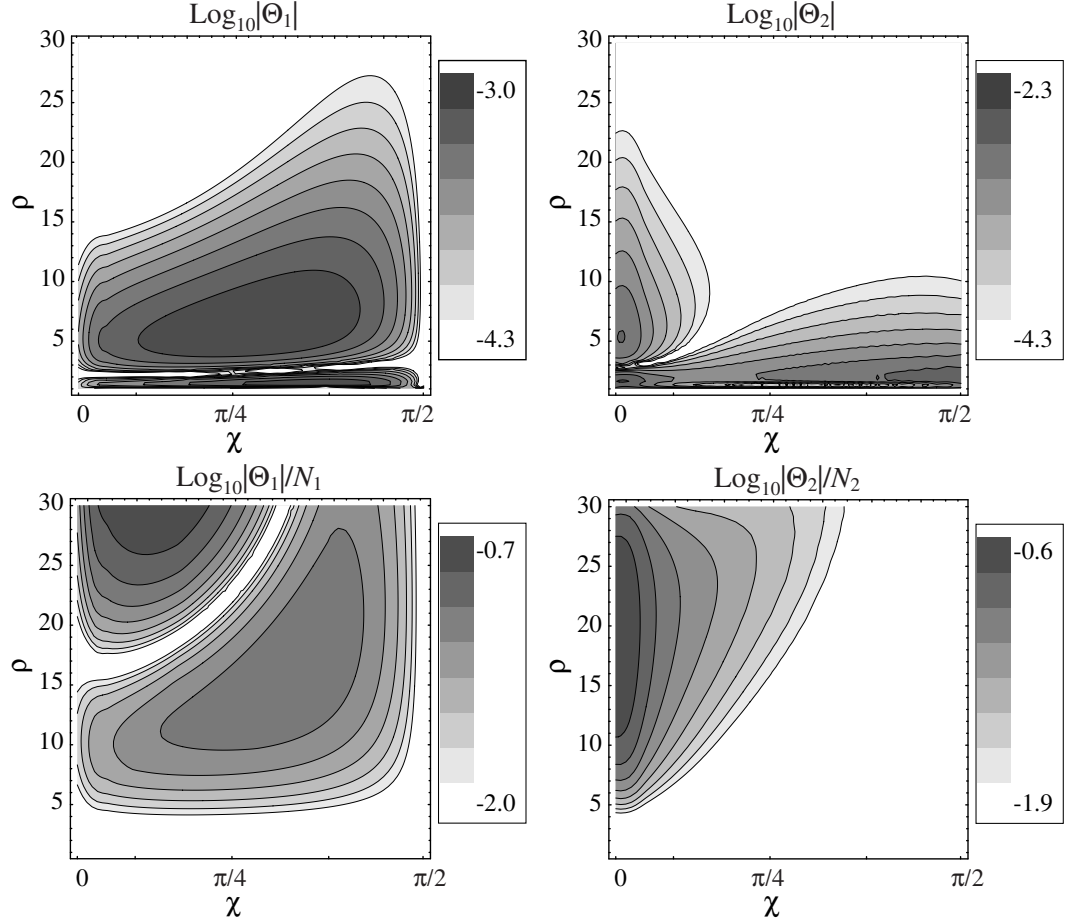


FIG. 4: An illustration of the constraint equations for  $L = 15$ . The figures that plot the absolute values of two constraint equations,  $|\Theta_1|$  and  $|\Theta_2|$ , show the absolute errors of the constraint equations. The other two figures plotting  $|\Theta_1(\rho, \chi)|/N_1(\rho, \chi)$  and  $|\Theta_2(\rho, \chi)|/N_2(\rho, \chi)$  show the relative accuracy of the constraint equations since  $N_1$  and  $N_2$  are norms of respective constraint equations (See the caption of Table I for the definition). As expected, the absolute errors of the constraint equations are observed mainly near the axis of polar coordinates and around the horizon. However, the relative accuracy is not significantly low around the horizon, but it is worse near the axis and in the asymptotic region.

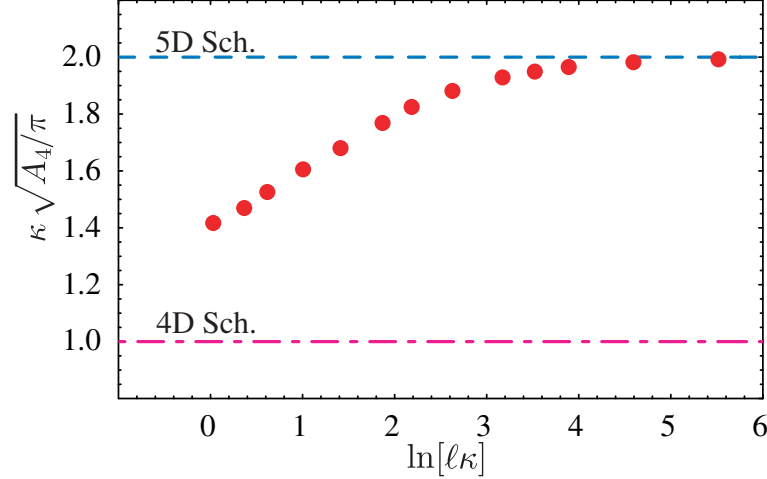


FIG. 5: Thermodynamic relation between the surface gravity  $\kappa$  and the 4D area  $A_4$ . Appropriate non-dimensional combinations are taken. The filled circles represent the numerical solutions for  $L = 3, 4, 5, 7, 10, 15, 20, 30, 50, 70, 100, 200$ , and  $500$ . For reference, we plotted the same thermodynamic relations for the 4D and the 5D Schwarzschild black hole. One clearly sees that the larger the parameter  $\kappa\ell$  becomes, the closer the numerical solutions lie to the line of the 5D Schwarzschild black hole. As  $\kappa\ell$  decreases, the solutions deviate from the line of the 5D Schwarzschild black hole and move toward that of the 4D Schwarzschild black hole.

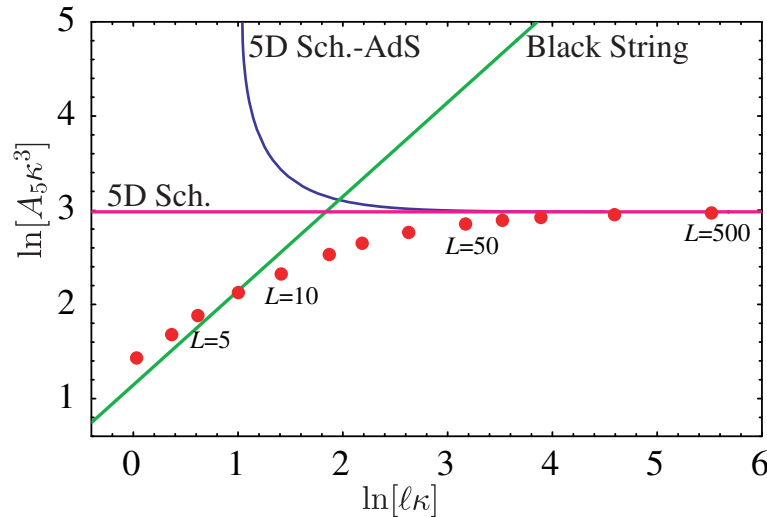


FIG. 6: Thermodynamic relation for the surface gravity  $\kappa$  and the 5D area  $A_5$  with an appropriate non-dimensional combination ( $L = 3 \sim 500$ ). Filled circles represent the results of numerical solutions. Thermodynamic relations for the 5D Schwarzschild, the 5D Schwarzschild-AdS and the black string are also plotted. A similar tendency as in Figure 5 is observed; as  $\ell\kappa$  is decreased, the numerical solutions deviate from the curve of the 5D Schwarzschild solution, and it approaches and crosses the line of the black string.

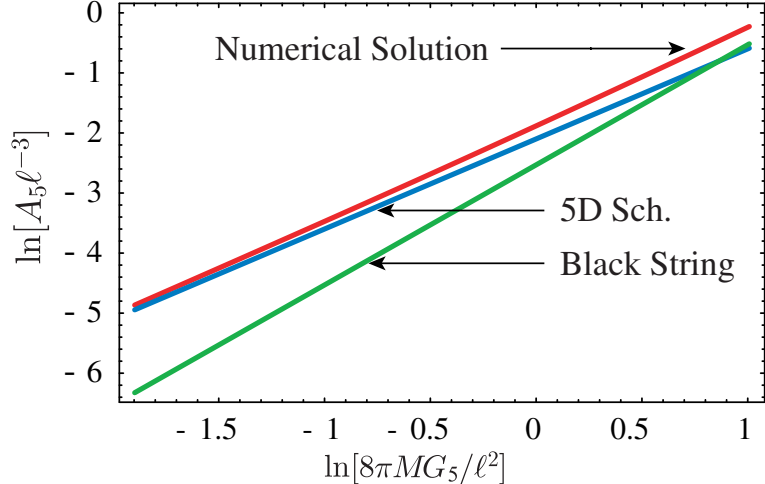


FIG. 7: Plot showing the relation between the thermodynamic mass and the entropy. The thermodynamic mass is calculated by using the first law of thermodynamics,  $dM = (\kappa/8\pi G_5)dA$ , where  $G_5$  is gravitational constant in five dimensions. The thermodynamic mass in the non-dimensional combination  $8\pi MG_5/\ell^2$  are  $3(\pi A_5/2\ell^3)^{2/3}$  and  $2\sqrt{\pi A_5/\ell^3}$  for the 5D Schwarzschild black hole and for the black string, respectively. Note that the entropy of the 5D Schwarzschild-AdS black hole is always smaller than that of the 5D Schwarzschild black hole of the same mass, although the difference is very small in the plotted region. The thermodynamic mass for the localized black hole is calculated using the solutions for  $L = 5 \sim 500$ . In computing the thermodynamic mass, the data points of  $\kappa$  and  $A_5$  are interpolated. This figure shows that the localized black hole has greater entropy, at least, in the plotted region than both the black string and the 5D Schwarzschild black hole of the same mass.

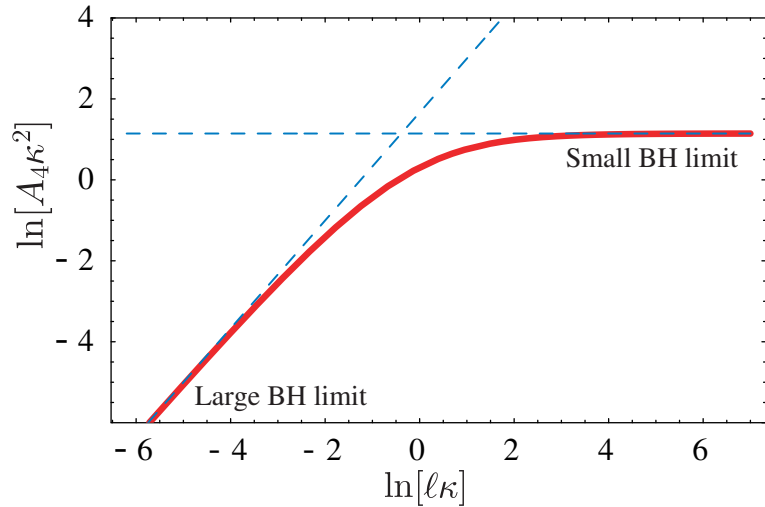


FIG. 8: This figure shows the thermodynamic relation for the EHM solution in the 4D braneworld model [29]. We can compare this relation with the numerical solution in the 5D braneworld model presented in Figure 6. The two dashed lines show the small and the large limit of black hole, which are given as  $A_4\kappa^2 = \pi$  and  $A_4\kappa^2 = (2^{7/3}\pi/3)(\kappa\ell)^{4/3}$ , respectively.

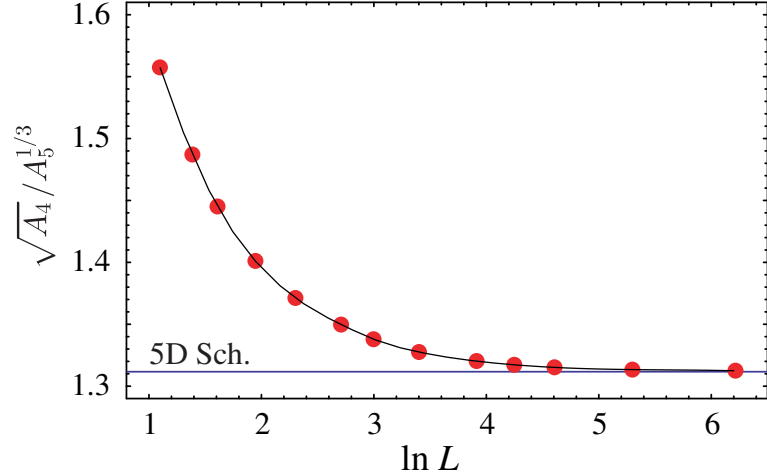


FIG. 9: An illustration of  $\sqrt{A_4}/A_5^{1/3}$ . This plot shows a degree of deformation of black hole. One sees that as  $L$  decreases the ratio of a mean radius in four-dimension  $A_4^{1/2}$  (on the brane) to that in five-dimension  $A_5^{1/3}$  increases. It indicates that the black hole tends to flatten as its horizon radius increases.

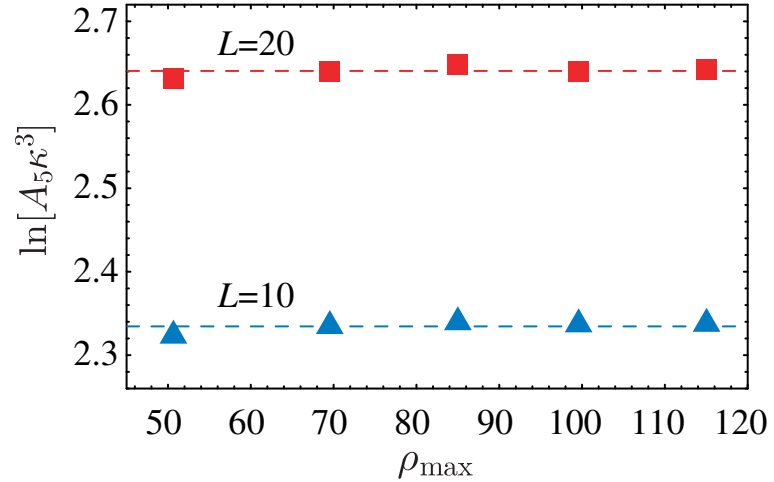


FIG. 10: A plot showing the sensitivity of the numerical solutions to the position of asymptotic boundary. The calculations are performed for  $L = 10$  and  $L = 20$ . The position of asymptotic boundary  $\rho_{\max}$  is changed from  $\rho_{\max} = 50$  to  $\rho_{\max} = 115$  keeping the ratio of the resolution fixed at  $\delta\rho_{\max}/\delta\rho_1 \approx 2.71$  with  $\delta\rho_1 \approx 0.05$ . We see that the variation of the thermodynamic quantity is no more than 1%, and is stable for this parameter range of  $\rho_{\max}$ .